Three Dimensional Flow Simulation in Yarn Duct of Interlacers with Various Cross-Sectional Shapes

Qiu Hua, Ph.D., Yan Jin

Jiangnan University, Textile and Clothing Institute, Wuxi, Jiangsu CHINA

Correspondence to:
Qiu Hua email: qiuhua@jiangnan.edu.cn

ABSTRACT
This goal of this paper was to determine the flow characteristics of compressible airflow in the yarn duct of an interlacer using numerical simulations to study the effects of cross-sectional shapes of yarn duct on the performance of interlacers. A CFD (Computational Fluid Dynamics) software package ANSYS CFX was used to calculate the flow patterns in the yarn duct. The relationship between the performance of the interlacer and the distribution of the velocity vector, the airflow speed and the particle trace of flow were examined in order to propose a better design of interlacers. From the results of the calculations, if the vortices on the middle cross-section of the yarn duct make the filaments revolve continuously, then a large number of entanglements can be achieved. The velocity at the central point of the yarn duct was the deciding factor as to a sufficient opening for the filaments. However, too high of a velocity makes the filaments stay on the wall, hindering them from entangling with each other.

Keywords: Interlacer, Cross-section, Yarn duct, CFD.

INTRODUCTION
DuPont invented interlacing technology in 1961 [1]. It can be used to improve the cohesion between multi-filament yarn, to facilitate winding-up and to produce novel yarn [2]. A basic type of interlacer is composed of two yarn guides ①, a yarn duct ② and an air jet nozzle ③ as shown in *Figure 1a*. Blowing compressed air onto a yarn running across the yarn duct causes the filaments to entangle and form interlaced yarn with intermittent entangling and openings. *Figure 1b* shows the picture of an interlaced yarn [3].

The interlacer is the key part in the interlacing process. Yarn interlacing is the result of the action of compressed air on a bundle of loose filaments; hence, the airflow patterns strongly affect the characteristics of the interlaced yarn and the performance of interlacer.

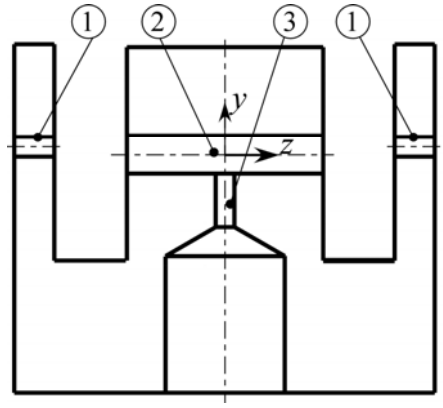

FIGURE 1. Interlacer and interlaced yarn.

Research has been carried out to clarify some airflow patterns, such as static pressure on the yarn duct [4-6] and dynamic pressure near the yarn duct [3], either by an experimental method [4, 5], a computational method or by the combination of these two methods [4, 7]. Most research paid a lot of attention to the measurement of the airflow patterns. However, little attention was paid to the relationship between the performance of the interlacer and the flow patterns. Furthermore, designing new types of interlacers typically requires the manufacture of interlacers and experimentation, which is time consuming and expensive.

In our previous study, seven interlacers with various cross-sectional shapes of yarn duct were made and then the effect on the characteristics of the interlaced yarn [8] and the yarn motion in the yarn duct [9, 10] was studied.

On the basis of our previous research [11], which aimed to find a useful way to simulate the airflow in the circular yarn duct, we calculated the airflow patterns in these seven interlacers with the commercial CFD software package ANSYS CFX. The objective of this research was to clarify the relationships between the performance of the interlacers and the flow patterns inside the yarn duct and discover a better way to design interlacers with a high performance level.

SIMULATION METHOD

The airflow patterns in seven yarn ducts were calculated with ANSYS CFX which was composed of five modules: Workbench, CFX-mesh, CFX-pre, CFX-solver and CFX-post [12]. *Figure 2* gives the process flow of ANSYS CFX.

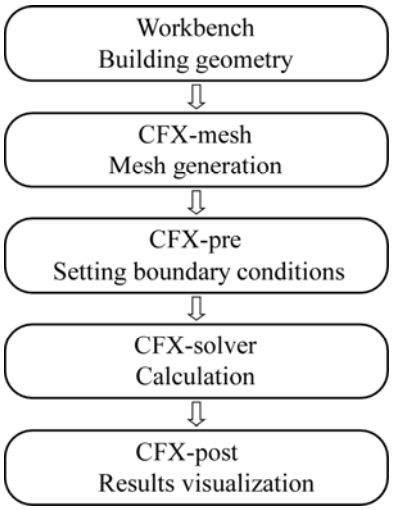

FIGURE 2. Process flow of ANSYS CFX.

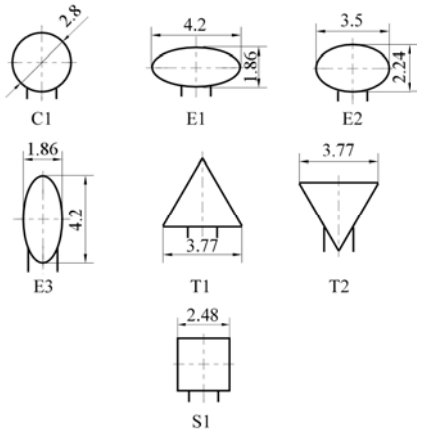

FIGURE 3. Cross-sectional shapes and sizes of yarn ducts (unit: mm).

The cross-sectional shapes and sizes of the yarn ducts are shown in *Figure 3*. The diameter of the air jet nozzle was 1.4 mm and the length of the yarn duct was 25.4 mm. Notation C1 represents the interlacer with a circular yarn duct. E1, E2 and E3 are interlacers with an elliptical yarn duct. S1 is a square yarn duct and T1 and T2 are triangular ones. For the sake of argument, the yarn ducts of C1, E1, E2 and E3 are regarded as round shapes and the others are cornered shapes.

Geometry Construction

Figure 4 shows the geometry built in the simulation (taking interlacer E2 as an example). In order to save time with the calculations, half of the original interlacer was considered due to the symmetrical nature of the interlacer. The geometry was comprised of three parts: an air jet nozzle, a yarn duct and an outer region. The diameter and length of the outer region were five times and twenty times the length of the diameter of the yarn duct, respectively. The outside region (the atmospheric region) of the cylindrical shape was added to the outside of the yarn duct as the flow geometry. The outside region was used to accurately set the boundary conditions at the infinity of the atmosphere in the ANSYS CFX. The notation (x, y, z) is the Cartesian coordinate system.

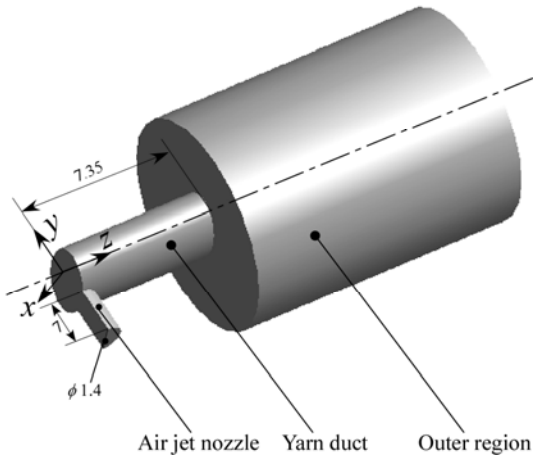

FIGURE 4. Geometry built in the simulation (unit: mm).

Mesh Generation

The numerical method used for discretization in CFX was FVM (finite volume method). This approach involved subdividing the entire flow geometry into finite control volumes using meshes [13]. *Figure 5* illustrates the distribution of the mesh elements on the plane z = 0 mm in the interlacer E2. The inflation layers on the yarn duct wall were created to ensure the accuracy of the simulation.

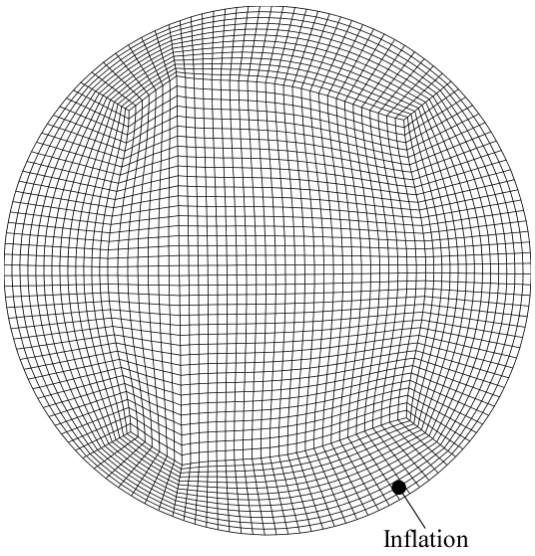

FIGURE 5. Distribution of mesh elements on plane z = 0 mm.

Boundary Conditions

Since these seven interlacers can produce the interlaced yarn with a large number of entanglements at a supplied air pressure $p_0 = 0.3$ MPa (gauge pressure) [9], the flow patterns in the yarn duct at that pressure were calculated. Moreover, because the interlacers E2 and T2 were superior to the other interlacers, in terms of the number and strength of entanglements, the flow patterns in their yarn ducts at p_0 = 0.2, 0.4 and 0.5 MPa were calculated.

The air of the working fluid was regarded as a viscous and compressible ideal gas. Since the Reynolds number in the yarn duct was an order of 10^7 [4], the airflow was turbulent and the standard $k-\varepsilon$ model was used in the simulation because it was more accurate and robust [7]. The following simultaneous governing equations for the conservation of mass, momentum and energy, the state, and the standard $k-\varepsilon$ turbulence model were solved by CFX-Solver [13].

Continuity equation:

$$\frac{\partial \rho}{\partial t} + \nabla \bullet (\rho \boldsymbol{U}) = 0 \tag{1}$$

Momentum equation:

$$\frac{\partial \rho \boldsymbol{U}}{\partial t} + \nabla \bullet (\rho \boldsymbol{U} \otimes \boldsymbol{U}) - \nabla \bullet (\mu_{eff} \nabla \boldsymbol{U}) = -\nabla p' + \nabla \bullet (\mu_{eff} \nabla \boldsymbol{U})^{\mathrm{T}} \tag{2}$$

Energy equation:

$$\frac{\partial (\rho h_{\mathrm{tot}})}{\partial t} - \frac{\partial p}{\partial t} + \nabla \bullet (\rho \boldsymbol{U} h_{\mathrm{tot}}) = \nabla \bullet (\lambda \nabla T) + \nabla \bullet (\boldsymbol{U} \bullet \boldsymbol{\tau}) + \boldsymbol{U} \bullet \boldsymbol{S}_{\mathrm{M}} + \boldsymbol{S}_{\mathrm{E}} \tag{3}$$

State equation:

$$p + p_{\mathrm{atm}} = \rho R T \tag{4}$$

Turbulence kinetic equation:

$$\frac{\partial (\rho k)}{\partial t} + \nabla \bullet (\rho \mathbf{U} k) = \nabla \bullet [(\mu + \frac{\mu_t}{\sigma_k}) \nabla k] + P_k - \rho \varepsilon \tag{5}$$

Turbulence dissipation equation:

$$\frac{\partial (\rho \varepsilon)}{\partial t} + \nabla \bullet (\rho \boldsymbol{U} \varepsilon) = \nabla \bullet [(\mu + \frac{\mu_t}{\sigma_\varepsilon}) \nabla \varepsilon] + \frac{\varepsilon}{k} (C_{\varepsilon 1} P_k - C_{\varepsilon 2} \rho \varepsilon) \tag{6}$$

where ρ is density, t time, U air velocity, μ_{eff} effective viscosity, p' modified pressure, h_{tot} total enthalpy, p static pressure (gauge pressure), λ thermal conductivity, T absolute temperature, $\boldsymbol{\tau}$ stress, S_M momentum source, S_E energy source, p_{atm} atmospheric pressure (=0.1013MPa), R universal gas constant, k turbulence kinetic energy, μ viscosity, μ_t turbulent viscosity, $\sigma_k, \sigma_\varepsilon, C_{\varepsilon 1}, C_{\varepsilon 2}$ constants, P_k shear production of turbulence and ε turbulence dissipation rate.

When the supplied air pressure p_0 (gauge pressure) was 0.2 - 0.6 MPa in the rectification tank, where the air velocity $v_0 = 0$ m/s and the absolute temperature $T_0 = 293$ K, the airflow choked in the air jet nozzle connected to the rectification tank. Hence, we could obtain the air velocity v_{ent}, the relative air pressure p_{ent} and an absolute temperature T_{ent} at the entrance of the air jet nozzle as shown in *Table I*. The symmetry boundary condition was used in the middle section z = 0 mm. No slip and adiabatic boundary conditions were applied on the wall of interlacer. The pressure and the temperature on the boundary of the outside region were 0 MPa and 293 K in the atmosphere, respectively. The yarn existence was ignored in the simulation because the cross-sectional area of the yarn duct was extremely larger than that of the yarn.

TABLE I. Boundary conditions at entrance of air jet nozzle.

In rectification tank			At entrance of air jet nozzle		
v_0 m/s	p_0 MPa	T_0 K	v_{ent} m/s	p_{ent} MPa	T_{ent} K
0	0.2 0.3 0.4 0.5	293	313.2	0.1591 0.2112 0.2647 0.3175	244.1

Since the yarn duct was very short and the speed of the compressed air very high, the interlacing process was completed in a very short time. For simplification, we assumed that the process was adiabatic, i.e., no heat transferred through the wall of the interlacer. On the wall of the yarn duct and air jet nozzle, no slip was applied.

Computational Scheme and Computer

The numerical technique utilized for discretization was UDS (upwind difference scheme). The number of iteration was set to 1000, which ensured the required level of convergence，RMS（root mean square of the residual）=1×10^5. The runs were performed on an Intel Xeon 2 CPU E5630 with a clock speed of 2.53 GHz and 12 GB of RAM.

RESULTS AND DISCUSSION

Performance of Interlacers

The performance of an interlacer was evaluated from the number and strength of entanglements of the interlaced yarn it produced. The number of entanglements N was defined as the tangling number in the interlaced yarn per meter. After measuring N, the same specimen was used to measure N_r, which represented the residual number of tangling parts in the interlaced yarn after the action of a load of 132 mN/tex for 3 min. The strength of the entanglements S defined as N_r / N was an index for the durability of the tangling parts. The raw yarn made of polyester multi-filament, 16.7 tex/48 filaments, was used as a testing material. For each interlaced yarn sample, three specimens were taken from different parts of the interlaced yarn package. The length of each specimen was 2 m measured at a tension of 2.97 mN/tex. A better interlacer could produce the interlaced yarn with large N and proper S [14].

Figure 6 shows the comparison of the performance of the seven interlacers at a supplied air pressure p_0 = 0.3 MPa, the yarn speed v = 200 m/min and the overfeed ratio F = 2% (experimental). Among them, the circular yarn ducts, C1, E1, E2 and E3, were good for yarn interlacing and cornered yarn ducts, T1, T2 and produced an interlaced yarn with a higher strength of entanglements, S1 being the poorest.

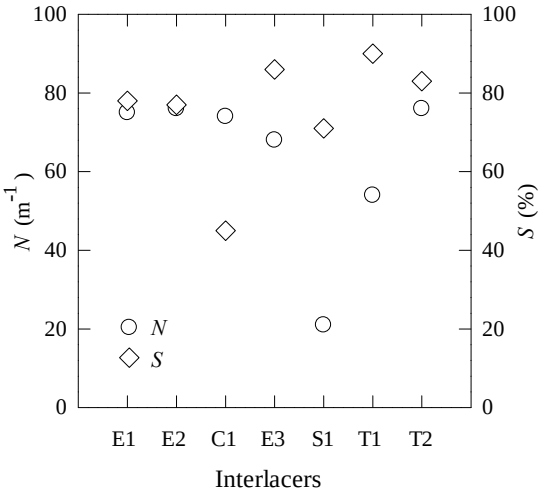

FIGURE 6. Comparison of performance of seven interlacers at p_0 = 0.3 MPa, v = 200 m/min and F = 2% (experimental).

Streamlines in Interlacer C1

Figure 7 shows the streamlines in half of the interlacer C1. When the airflow, from the air jet nozzle, goes into the yarn duct, the channel for the airflow was suddenly widened. As a result, in the vicinity of the center of the yarn duct on the symmetry plane, the supersonic airflow appeared. The pattern of the streamlines in the other 6 interlacers was similar to that in interlacer C1.

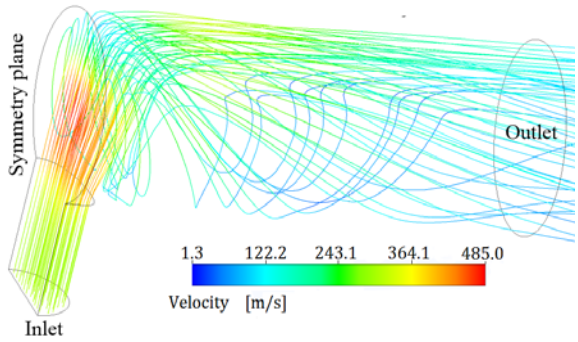

FIGURE 7. Streamlines in half part of the interlacer C1.

Air Velocity Vectors on the Plane Z = 0 Mm

The compressed air issued from the air jet nozzle acted directly on the yarn on the plane z = 0 mm. The yarn motion on the plane z = 0 mm characterized the yarn interlacing. Since the yarn was light, the flow

patterns on the plane z = 0 mm greatly affected the yarn motion.

Figure 8 shows the velocity vectors on the plane z = 0 mm in the interlacers E2, E3, T1 and S1 at $p_0 = 0.3$ MPa. Before the interlacing process, the yarn position was along the z axis and intersected the axis of air jet nozzle (y = 0). The flow patterns on the cross-section of yarn duct, including the axis of air jet nozzle, decided both the yarn motion and the spacing for the yarn interlacing.

From *Figure 8*, in the interlacer E2, the symmetric vortices appeared on the plane z = 0 mm, which offered a big space for revolving and interlacing the yarn. So the interlacer E2 produced the interlaced yarn with a large number of entanglements. In the interlacer E3, since the width of yarn duct was close to the diameter of air jet nozzle, no obvious vortices appeared. The yarn was difficult to run to the lower part of the yarn duct and could not be interlaced sufficiently because of the reverse flows on the plane z = 0 mm were weak.

In the interlacer T1, the vortices at the bottom of the yarn duct had little effect on the yarn motion because high speed flow directly blew yarn to the upper part of the interlacer. Hence, the filaments were trapped in that place for a long time and a small number of entanglements were produced.

In the interlacer S1, the vortices occured in the lower corner regions, where the speed of the flow was lower. The filaments were trapped and stayed in those regions and it was difficult for them to revolve. Therefore, the interlacer S1 had the poorest performance.

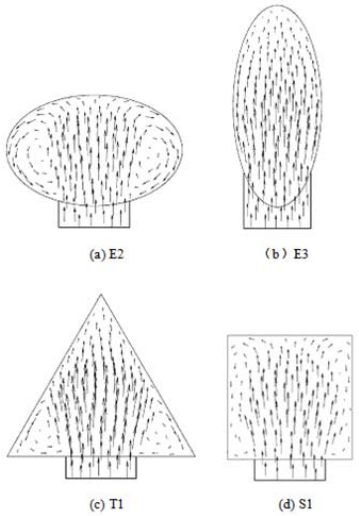

FIGURE 8. Velocity vectors on the plane z = 0 mm in the interlacers E2, E3 T1 and S1 at $p_0 = 0.3$ MPa.

Air Speed at Coordinate Origin

It is a known fact that effectively opening yarn is essential to good yarn interlacing. Since the yarn opening was performed by the action of compressed air, it was strongly affected by the U_{y0} which was defined as the y component of air velocity at the coordinate origin (0,0,0). *Figure 9* shows U_{y0} in the seven interlacers at $p_0 = 0.3$ MPa. Among these seven interlacers, U_{y0} in interlacers C1, E2 and T2 were higher and close to each other. In interlacers E1, E3, T1 and S1, U_{y0} were lower, especially in T1. In these cases, the yarn could not be opened sufficiently and a small number of entanglements were produced.

Speed in the *Y* on Initial Yarn Position

The y component of the air velocity was denoted by U_y. *Figure 10* shows the distribution of U_y on the z axis in the interlacers C1, E2 and T2. These interlacers were chosen because they could effectively open the yarn at the origin position (0, 0, 0). As shown in the figure, U_y decreased sharply in the region z = 0 - 2 mm and then close to 0 m/s, which meant that the yarn was mainly opened in the middle part of the yarn duct. Designing the interlacers with a higher U_y on the initial yarn position is important to improve the number of entanglements.

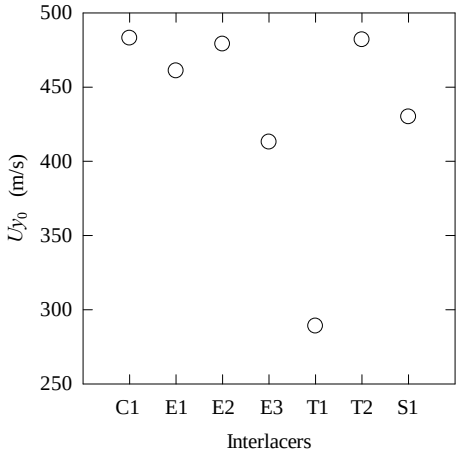

FIGURE 9. U_{y0} in seven interlacers at $p_0 = 0.3$ MPa.

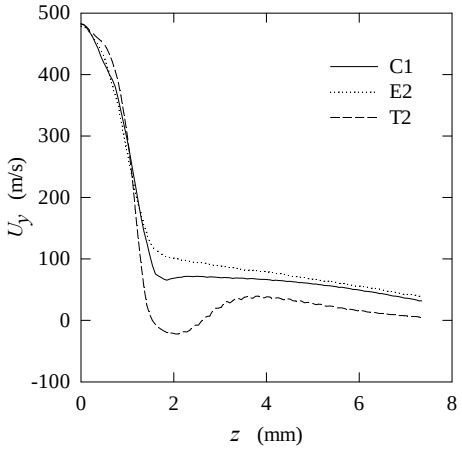

FIGURE 10. Distribution of U_y along the z axis in the interlacers C1, E2 and T2.

Flow Patterns in the Interlacers E2 and T2

Interlacers E2 and T2 are superior to the other interlacers when both the number and strength of entanglements were considered. They could produce the interlaced yarns with a larger N at the moderate supplied air pressure $p_0 = 0.3$ MPa, not at 0.2 nor 0.5 MPa. *Figure 11* shows the relation between p_0 and U_{y0} in the interlacers E2 and T2. From the figure, U_{y0} increased with p_0 since the opening of the yarn improved, the number of entanglements also increased. But from the previous study [9], the interlacer E2 and T2 produced the interlaced yarn with a smaller number of entanglements at $p_0 = 0.5$ MPa.

Figure 12 shows the distribution of the static pressure p_s on the inner yarn duct wall of the interlacer E2 at the plane z = 0 mm. *Figure 13* shows the distribution of p_s on the upper yarn duct of the interlacer T2 at z = 0 mm. The coordinate axis θ on the plane z = 0 mm was defined in *Figure 14*. From *Figures 12* and *13* p_s increased with p_0 and reached the maximum at the extension of the axis of air jet nozzle, which made the yarn stay near the top or upper wall of the yarn duct for a long time and hindered the yarn from continuously revolving.

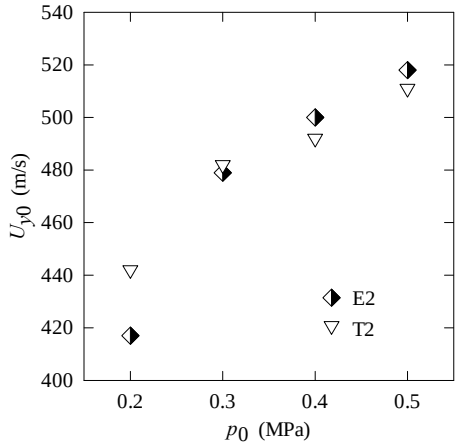

FIGURE 11. Relation between p_0 and U_{y0} in the interlacers E2 and T2.

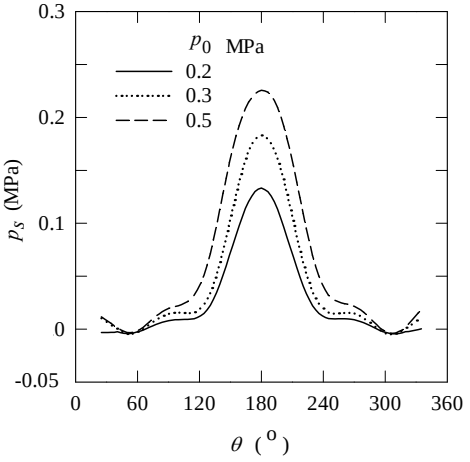

FIGURE 12. Distribution of p_s on yarn duct wall of the interlacer E2 at z = 0 mm.

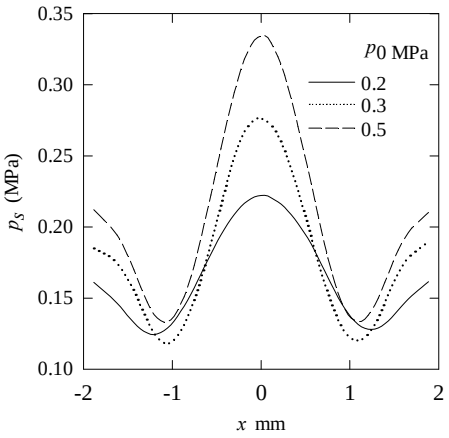

FIGURE 13. Distribution of p_s on the yarn duct wall of the interlacer T2 at z = 0 mm.

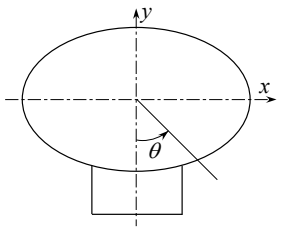

FIGURE 14. Definition of coordinate axis θ on the plane z = 0 mm.

CONCLUSIONS

In this study, the flow patterns in the seven interlacers with various cross-sectional shapes of yarn ducts were calculated with CFD software package ANSYS CFX. The performance of the interlacer was decided by the flow patterns in its yarn duct.

(1) Vortices at the plane z = 0 mm affected the space for yarn interlacing.

(2) The y component of air velocity U_y affected the yarn interlacing. Higher U_y was good for the yarn opening and interlacing.

(3) Higher supplied air pressure p_0 was good for the yarn opening. However, too high p_0 would blow the filaments near the wall of yarn duct where they stayed, which decreased the number of entanglements.

(4) In practice, the interlacers E2 and T2 could be used to produce the interlaced yarns with a higher number of entanglements and the interlacer T2 could be used to produce higher strength entanglements.

ACKNOWLEDGMENT

The authors are grateful for the financial supported by the Fundamental Research Funds for the Central Universities (No.JUSRP30906) and the Open Project Program of Key Laboratory of Eco-Textiles, Ministry of Education, Jiangnan University (KLET1014).

REFERENCES

[1] Y Iemoto, S Chono & K Sawazaki, *Journal of the Textile Machinery Society of Japan*, 35(1989)1-5.

[2] A Dernir, *Textile Asia*, 21(1990)114-122.

[3] Y Iemoto, T Shuichi & J Lu, *Journal of Textile Engineering*, 55(2009)111-118.

[4] K Murakami and K Tokunaga, *Journal of Textile Engineering*, 52(2006)73-79.

[5] Y Iemoto, S Chono, H Qin & W Lou, *J. Text. Mach. Soc. Japan*, 46(2000).

[6] Y Iemoto and S Chono, *J. Text. Mach. Soc. Japan*, 43(1997)38-46.

[7] K Tokunaga and K Murakami, *Journal of Textile Engineering* (2006)121-129.

[8] H Qiu, Y Iemoto & S Tanoue, *Journal of Textile Engineering*, 53(2007)1-8.

[9] H Qiu, Y Iemoto & S Tanoue, *Journal of Textile Engineering*, 53(2007)59-67.

[10] H Qiu and M Ge, *Journal of Donghua University (Eng. Ed.)*, 27(2010)775-780.

[11] Y Iemoto and H Qiu, *Journal of Textile Engineering*, 56(2010)87-96.

[12] ANSYS, *ANSYS Introduction*, ANSYS, Inc., Canonsburg, (2005)7-13.

[13] ANSYS, *ANSYS CFX-Solver Theory Guide*, ANSYS, Inc., Canonsburg, (2005)22-24.

[14] H Qiu and M Ge, *FIBRES & TEXTILES in Eastern Europe*, 18(2010)26-29.

AUTHORS' ADDRESSES

Qiu Hua, Ph.D.
Yan Jin
Jiangnan University
Textile and Clothing Institute
Lihue Road 1800#
Wuxi, Jiangsu 214000
CHINA